



Article

Fabrication of Conjugated Porous Polymer Catalysts for Oxygen Reduction Reactions: A Bottom-Up Approach

Sujoy Bandyopadhyay^{1,2}, Su Ryong Ha³, M. Alam Khan³, Cheongbeom Lee³, Hong In Jeong³, Snehal Lokhandwala¹, Mohaseen S. Tamboli³ , Bo Ram Lee⁴, Danil W. Boukhvalov^{5,6} and Hyosung Choi^{3,*} 

¹ Department of Chemistry, SRICT Institute of Science & Research (SRICT-ISR) Block No. 402, Ankleshwar-Valia Road, Ta: Valia, Bharuch 393135, India; sujoyb9@gmail.com (S.B.); snehal.lokhandwala@sRICT.in (S.L.)

² Department of Chemistry, Indrashil University, Rajpur, Gujarat 382740, India

³ Department of Chemistry and Research Institute for Natural Sciences, Hanyang University, 222 Wangsimni-ro, Seongdong-gu, Seoul 04763, Korea; ashenvale@hanyang.ac.kr (S.R.H.); alamkhan77@gmail.com (M.A.K.); latine@hanyang.ac.kr (C.L.); jhi3343@hanyang.ac.kr (H.I.J.); tamboli.mohseen@gmail.com (M.S.T.)

⁴ Department of Physics, Pukyong National University, 45 Yongso-ro, Nam-Gu, Busan 48513, Korea; brlee@pknu.ac.kr

⁵ College of Science, Institute of Materials Physics and Chemistry, Nanjing Forestry University, Nanjing 210037, China; 2018170@njfu.edu.cn

⁶ Institute of Physics and Technology, Ural Federal University, Mira Street 19, 620002 Yekaterinburg, Russia

* Correspondence: hschoi202@hanyang.ac.kr; Tel.: +82-2-2220-2619; Fax: +82-2-2298-0319

Received: 13 September 2020; Accepted: 12 October 2020; Published: 22 October 2020



Abstract: The present study demonstrates the fabrication of a conjugated porous polymer (CPP-P2) through a Pd-catalyzed Suzuki–Miyaura poly-condensation reaction. ¹³C cross-polarization solid-state NMR and Fourier transform infrared (FTIR) spectroscopy were used to characterize CPP-P2. Pristine nitrogen-containing CPP was explored as a catalyst for the oxygen reduction reaction in 0.1 M KOH aqueous alkaline media. In the case of CPP-P2, the polymer oxygen reduction reaction occurs via a four-electron transfer mechanism. An understanding of the oxygen reduction at the molecular level and the role of molecular packing in the three-dimensional structure was proposed based on density functional theory (DFT) modeling.

Keywords: conjugated porous polymer catalysts; Suzuki–Miyaura poly-condensation reaction; oxygen reduction reaction

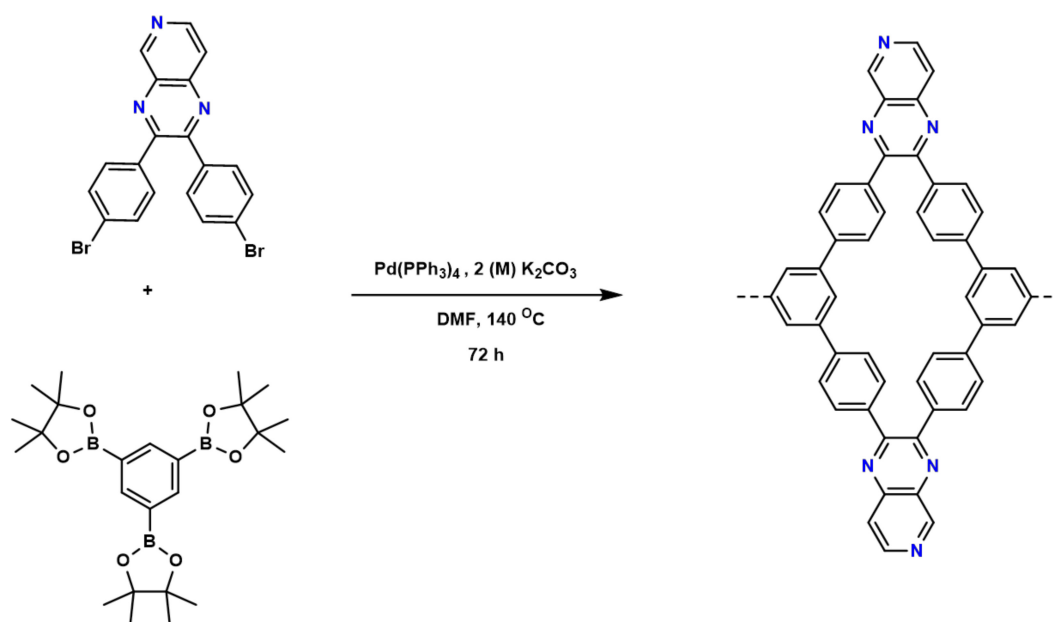
1. Introduction

Escalating demand for developing clean and renewable energy sources, next-generation energy conversion, and storage systems is being generated to mitigate an energy crisis in the 21st century. Due to the high theoretical energy density and the environmentally benign nature of several electrochemical devices, the fuel cell is one of the most important technological and scientific devices [1]. In this context, the electrocatalytic reduction of oxygen to water is a key step in fuel cells [2]. To date, platinum-supported carbon is considered the most efficient catalyst for the oxygen reduction reaction (ORR); however, the high cost of platinum and its low tolerance and poor stability in methanol have proven to be major obstacles for the commercialization of this technology [3]. Over the last few decades, various transition metal-based electrocatalytic methods have also been developed for

the ORR, but these metals undergo corrosion loss [4,5]. Recently, endeavoring to overcome these challenges, many research groups have developed organo-electrocatalysts as alternatives to platinum carbon [6–10]. Nitrogen-doped carbon materials, as metal-free catalysts, have high electrocatalytic activity for the ORR and good tolerance in methanol, even under acidic conditions [11]. However, carbon-based materials such as heteroatom-doped porous carbon, functionalized carbon nanotubes (CNTs), and nitrogen-doped graphene have frequently been used for the platinum-free electrocatalysis of the ORR [12]. Among these catalysts, conjugated porous organic polymer (CPP) materials play a crucial role in the design of efficient and promising ORR electrocatalysts due to their highly cross-linked porous 3D structure with a nitrogen functional group that provides a scaffold for improved interactions between oxygen and the nitrogen functional group of the polymer [13–18]. In particular, nitrogen-containing CPPs have emerged as highly active oxygen reduction electrocatalysts, resulting in a high reaction current and providing good tolerance in methanol [13]. Recently, we reported the fabrication of a 2,3-bis(4-bromophenyl)pyrido(3,4-b)pyrazine (BPP)- and triethynylbenzene (TEB)-based CPP-P1 using a Sonogashira–Hagihara palladium-catalyzed cross-coupling reaction. The solid polymer was found to be a potential electrocatalyst for the ORR [19]. To understand the reduction process for the ORR in the present study, a new polymer was synthesized using 2,3-bis(4-bromophenyl)pyrido(3,4-b)pyrazine and 1,3,5-phenyltriboronic acid tris(pinacol)ester via a Suzuki–Miyaura poly-condensation reaction. Density functional theory (DFT) calculations exploring the mechanistic details of the ORR with the new CPP-P2 were additionally employed.

2. Results and Discussion

CPP-P2 polymer synthesis involved a multi-step process (Supporting Information, Scheme S1). First, the monomer was synthesized via a Schiff base reaction using pyridine-3,4-diamine and 1,2-bis(4-bromophenyl)ethane-1,2-dione. Next, the monomer 2,3-bis(4-bromophenyl)pyrido(3,4-b)pyrazine was reacted with the co-monomer 1,3,5-phenyltriboronic acid tris(pinacol)ester using palladium as a catalyst. A schematic illustration of the fabrication of a conjugated porous polymer (CPP-P2) from 2,3-bis(4-bromophenyl)pyrido(3,4-b)pyrazine and benzene-1,3,5-triboronic acid is shown in Scheme 1.



Scheme 1. Schematic illustration of the fabrication of a conjugated porous polymer (CPP-P2) from 2,3-bis(4-bromophenyl)pyrido(3,4-b)pyrazine and benzene-1,3,5-triboronic acid.

CPP-P2 was thoroughly characterized by Fourier transform infrared (FTIR) spectroscopy, solid state ^{13}C cross-polarization magic angle spinning NMR spectroscopy, thermogravimetric analysis (TGA), field emission scanning electron microscopy (FESEM), and N_2 sorption experiments at 77 K. The Fourier-transform infrared (FTIR) spectroscopy of CPP-P2 was performed using Potassium bromide (KBr) pellets of the sample with a Perkin-Elmer FTIR instrument. Fifteen scans were signal-averaged, with a resolution of 8 cm^{-1} at ambient temperature. The FTIR spectra were used to better understand the structure of the solid polymer CPP-P2. As shown in Figure 1, characteristic aromatic C-H stretching at $\sim 3050\text{ cm}^{-1}$ originating from the aromatic building blocks was observed. The standard FTIR spectrum showed an aromatic group of methyl extending to 2926, 3034, and 3063 cm^{-1} [20]. An aromatic C=C stretching band was observed at 1605 cm^{-1} . A band near 1575 cm^{-1} was attributed to C=N stretching [21].

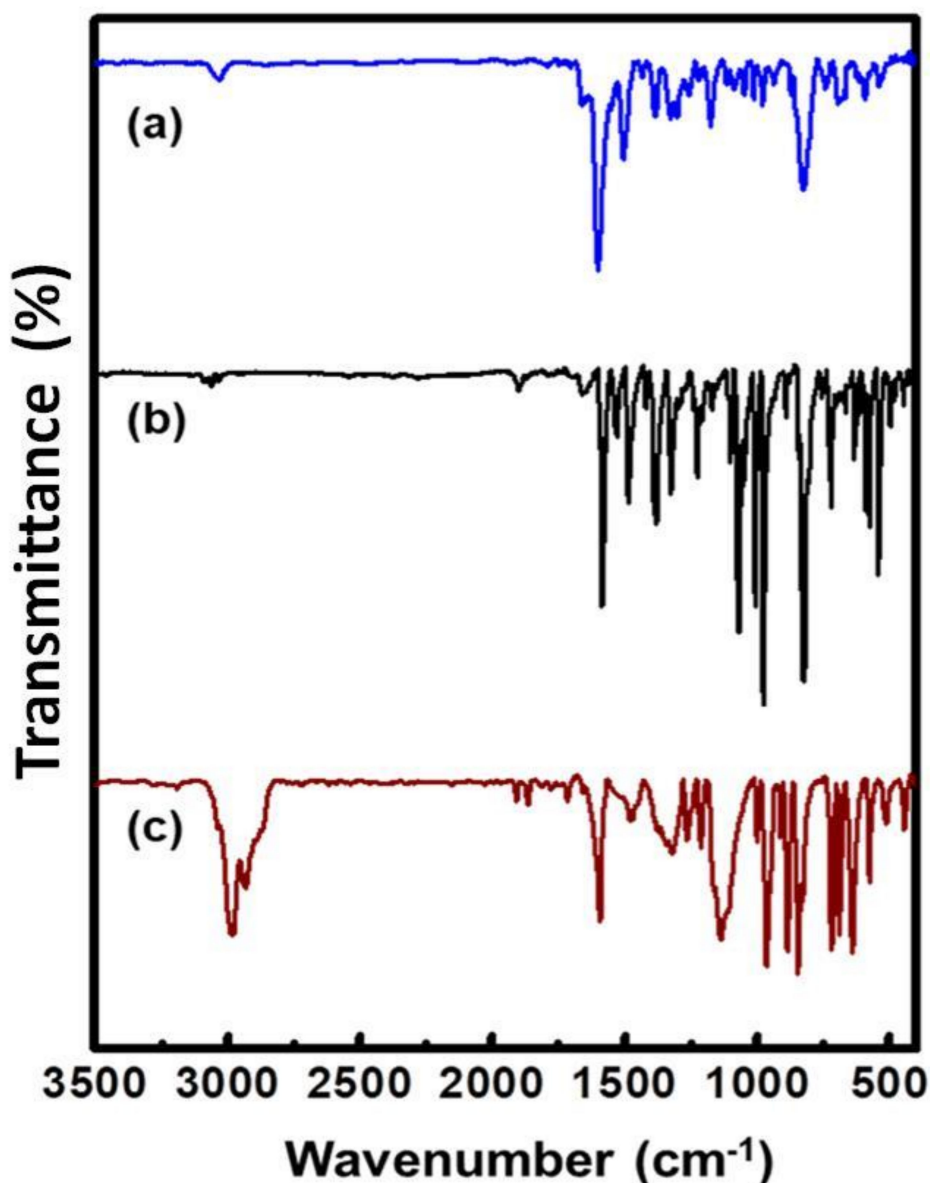


Figure 1. FTIR spectra of (a) CPP-P2, (b) 2,3-bis(4-bromophenyl)pyrido(3,4-b)pyrazine, and (c) benzene-1,3,5-triboronic acid.

Solid state ^{13}C NMR experiments were performed on a JEOL ECX 400 MHz (field 9.4 T) standard bore spectrometer equipped with a 4 mm solid-state magic-angle spinning MAS probe. The solid

samples were packed and spun at 8 kHz at the magic angle in the ^{13}C cross-polarization total suppression of spinning sidebands (CP-TOSS) NMR spectroscopy. The peak region of 120 to 160 ppm in Figure 2 revealed both aromatic C=C and C=N bonds of 2,3-bis(4-bromophenyl)pyrido(3,4-b)pyrazine and 1,3,5-phenyltriboronic acid tris(pinacol)ester.

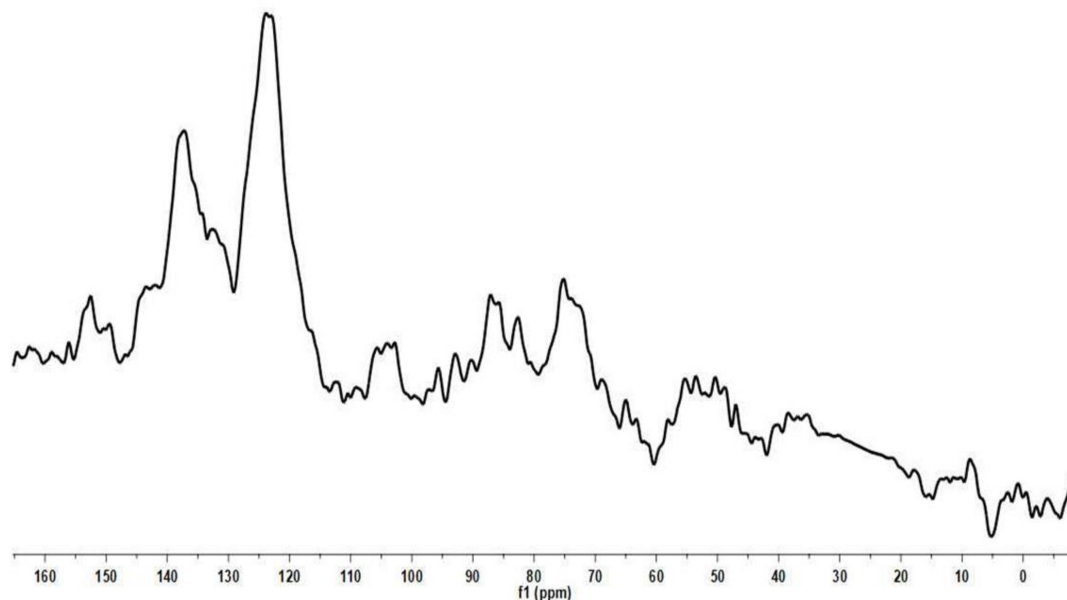


Figure 2. Solid state ^{13}C NMR spectrum of CPP-P2.

Furthermore, the thermal stability of CPP-P2 was assessed by TGA with a ramping rate of $10\text{ }^\circ\text{C}$ under a nitrogen atmosphere. As shown in Figure 3a, some initial weight loss was observed up to $150\text{ }^\circ\text{C}$, due to the dimethylformamide (DMF) solvent, after which the polymer was stable, which indicates that the polymer (CPP-P2) has high thermal stability. The morphology of CPP-P2 was analyzed by FESEM. Samples for microscopy were prepared by dropping ($\sim 0.2\text{ mg}$) polymer (powdered form) on an aluminum stub with a silicon wafer covered with adhesive carbon tape. All samples were coated with a thin layer of sputtered platinum prior to imaging. FESEM was carried out using an accelerating voltage of 15 kV. The FESEM image of CPP-P2 (Figure 3b) showed a granular morphology. The surface area of the polymer CPP-P2 was determined using nitrogen gas adsorption–desorption measurements carried out at 77 K. The polymer was dried at $100\text{ }^\circ\text{C}$ for 24 h under a high vacuum before the analysis. The Brunauer–Emmett–Teller (BET) surface area of CPP-P2 was approximately $65\text{ m}^2\text{ gm}^{-1}$. We determined the pore size to be 3.4 nm, which indicates that it is a mesoporous material.

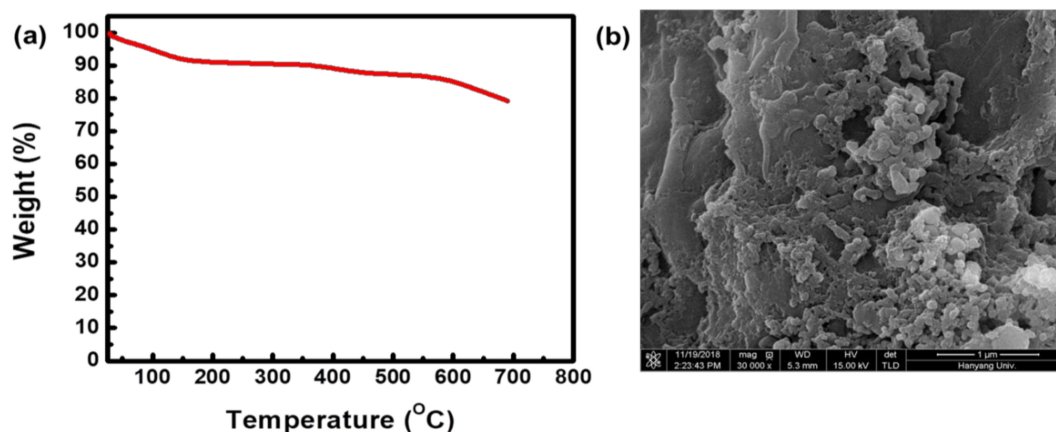


Figure 3. (a) Thermogravimetric analysis of CPP-P2; (b) FESEM of CPP-P2.

Cyclic voltammetry (CV) estimations were performed in a 0.1 M fluid KOH arrangement to examine the electrocatalysis property of CPP-P2, where solid polymer was stacked on glassy carbon and a graphite rod and Ag/AgCl (3.0 M KCl) were used as a working electrode, and counter and reference electrodes, respectively. In an O₂-saturated 1 M aqueous KOH solution, a clear peak was observed at -0.07 V (vs. Ag/Ag⁺), indicating oxygen reduction. We also conducted a control experiment in which a nitrogen-saturated 0.1 M aqueous KOH solution was utilized as the electrolyte, but no reduction peak was observed, as shown in Figure 4. Therefore, CPP-P2 had potential as a catalyst for the ORR. We conducted linear sweep voltammetry (LSV) at distinct rotation speeds (500–2500 rpm), as shown in Figure 4b, to further estimate the ORR catalyst potential. The CPP-P2 polymer exhibited phenomenal electrocatalytic activity, with an initial potential of -0.05 V (vs. Ag/Ag⁺) and an ORR current density of 3.59 mA cm⁻² at 2500 rpm. The half wave potential of the CPP-P2 polymer is -0.122 V with respect to the (Ag/Ag⁺) electrode. Utilizing the Koutecký–Levich equation, we determined the number of electrons transferred per oxygen molecule. The number of electrons transferred (n) in the oxygen reduction reaction process with the CPP-P2 polymer was determined to be 3.72 (considering $n = 4$ for Pt/C) (Figure 5), suggesting the prepared ORR catalyst has a four-electron pathway.

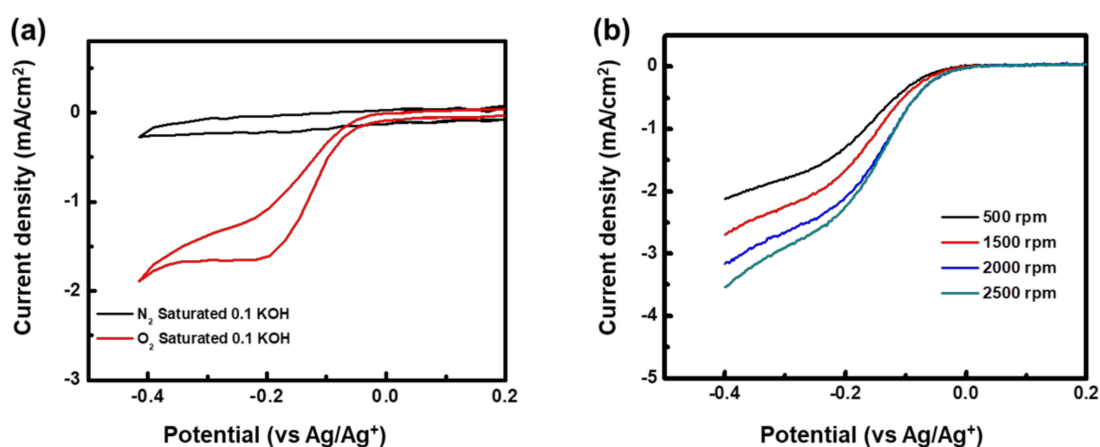


Figure 4. (a) Cyclic voltammograms for CPP-P2 under N₂-saturated and O₂-saturated 0.1 (M) KOH electrolyte. (b) Linear sweep voltammograms observed under different rotation speeds for the glassy carbon electrode for CPP-P2.

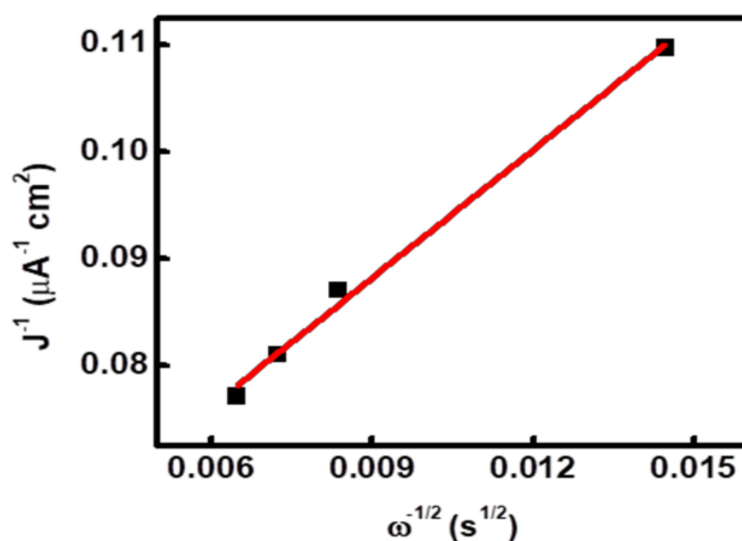


Figure 5. Koutecký–Levich plots of CPP-P2.

To determine the nature of these processes at the molecular level, we performed a first-principles modeling of the ORR in two model systems. For the modeling, we used a realistic chemical structure of CPP-P2. The polymer structure of the test materials was considered by introducing periodic boundary conditions. To make the model more comprehensive, we considered two structures (Figure 6) corresponding to different types of packing of the molecules inside the cells. Similar to the naming of the layered structure stacking, we further named the structure with molecules located one above another AA (Figure 6c) and the structure where the polymer chains shifted along the translation AB (Figure 6a,b). The results of the atomic structure calculations provided evidence that the type of packing significantly influenced the atomic structure of the central portion of the molecules. A comparison of these two structures provided an evaluation of the role of the environment in catalytic activity.

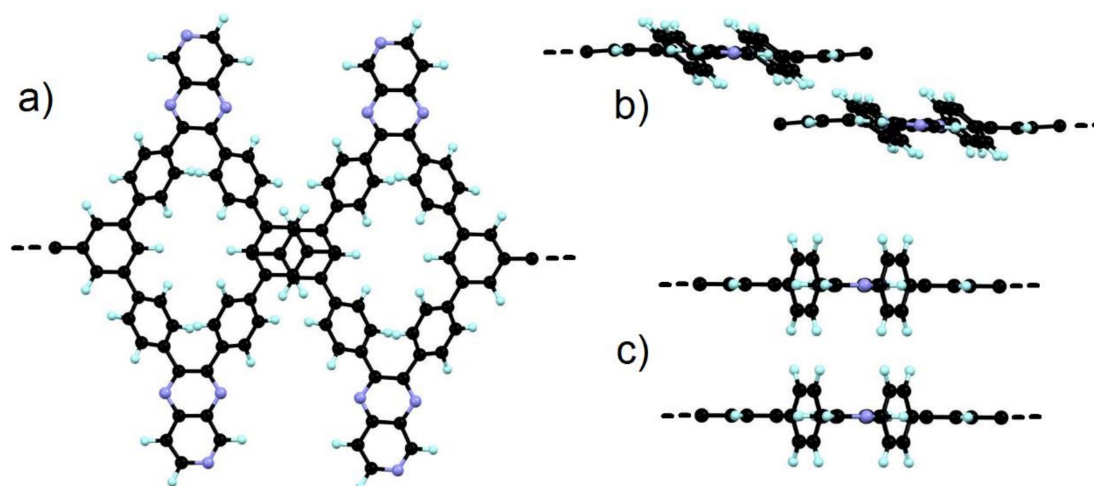
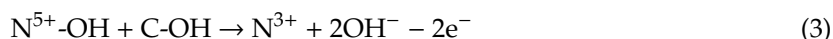
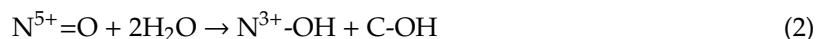


Figure 6. Atomic structures of (a,b) AB and (c) AA packing of the molecules within periodic boundary conditions. The bonds between the molecules in polymeric chains are shown by dashed lines.

Similar results from the modeling in our previous work demonstrates the most prevailing pathway for the oxygen reduction reaction in alkaline media with the formation of $^{\ast}\text{-OOH}$ and $^{\ast}\text{-O}$ groups being extremely energetically unfavorable, as these steps require unnatural N^{4+} for the above-studied catalyst. Therefore, we considered a further reaction pathway in which both pyrazine and pyridine groups can participate: detail of the mechanism is shown below (see Figure 7b,c).



Because the free energy calculated for the ORR suggests a significant (about 0.5 eV) preference of pyrazine for active sites, we discuss only the process that includes pyrazine sites. In order to verify the possibility, for the first step of the reaction, we performed calculations of the energies of the physical adsorption of an oxygen molecule on the ring with pyrazine groups and the activation energy (see Figure 7a). The energies of physical adsorption over the center of the considered hexagon is -0.61 eV for AA stacking and -0.64 eV for AB stacking. These numbers evidence a robust preferability of physical adsorption over these sites. The calculated values of the activation energies are $+1.16$ eV for AA stacking and $+0.96$ eV for AB stacking. Note that these values are close to the same values calculated for oxygen activation on pure graphene [22] and close to the values obtained for nitrogen-doped graphene, which demonstrates outstanding catalytic performance [23]. The causes of these moderate energy costs of the oxygen activation are the rather short distance between the nitrogen centers (0.284 nm, which is

close to the Pt–Pt distance, 0.277 nm) and possibility of covalent bond reconstruction to avoid the appearance of dangling bonds (Figure 7a).

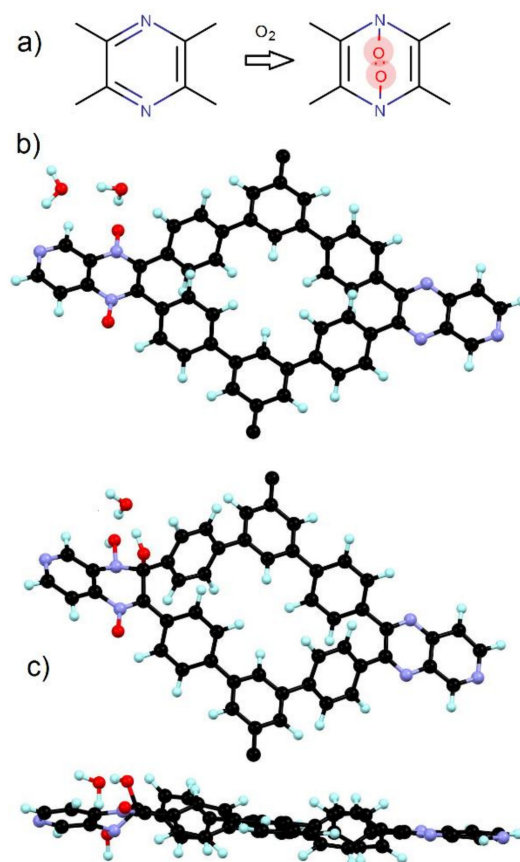


Figure 7. The scheme of bond reconstruction during activation of oxygen molecule on CPP-2 (a) and optimized atomic structures of the part of CPP-2 in the first (b) and second (c) steps of the reaction.

The natural ability of nitrogen atoms to change from the 3^+ oxidation state to 5^+ by the formation of double bonds with oxygen atoms in the first step of the reaction (Figure 7a) and two hydroxyl groups in the second step (Figure 7b) is used in this pathway. Note that the enthalpy of this first step is -1.49 eV for AB stacking and -2.09 eV for AA stacking (see Figure 8). The higher magnitude of the free energy of the first step overcomes the above-discussed energy cost of oxygen activation. In the second and fourth steps, water decomposition takes place, allowing hydrogen to interact with the N=O and hydroxyl groups, which get adsorbed at the nearest carbon site (Figure 7b). This transforms the C–N bond from a double bond to a single bond. The formation of these hydroxyl groups provides a visible distortion of the large part of the molecule (Figure 7a). The energy cost of the distortions depends on the rigidity of the molecular backbone and van der Waals interactions between different polymer chains. In the case of AB stacking, there are fewer Van der Waals interactions, especially in the area of the active part of the molecules (Figure 7a) and initial distortion of the molecular backbone (Figure 7b), which significantly decreases the energy cost of these steps of the ORR. In the third and fifth steps, the desorption of both hydroxyl groups takes place simultaneously. Note that the maximal energy cost of this step (~ 1.1 eV for AA stacking) is smaller than that for Au (001) surface in alkaline media (~ 1.8 eV) [24] and comparable with the values of the energy cost or ORR in acidic media for Pt (~ 0.4 eV) [25]. Steps 4 and 5 use another oxidized nitrogen atom, for producing a four-electron reaction (Figure 8), which is achieved by repeating Step 2 and Step 3.

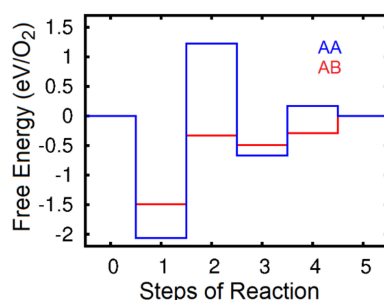


Figure 8. Free energy diagram of the steps of oxygen reduction reaction (ORR) in alkaline media for two different types of stacking of CPP-P2.

3. Experimental Section

3.1. Synthesis of 2,3-Bis(4-bromophenyl)pyrido(3,4-b)pyrazine

2,3-bis(4-bromophenyl)pyrido(3,4-b)pyrazine was synthesized following the reported procedure [19].

3.2. Synthesis of the CPP-P2

The CPP-P2 polymer was synthesized by a palladium-catalyzed Suzuki–Miyaura cross-coupling poly-condensation reaction between the monomer 2,3-bis(4-bromophenyl)pyrido(3,4-b)pyrazine (BPP) and co-monomer 1,3,5-phenyltriboronic acid tris(pinacol)ester. In a typical synthetic procedure, BPP (1 mmol), 1,3,5-phenyltriboronic acid tris(pinacol)ester (2 mmol), and tetrakis(triphenylphosphine) palladium (0) (10 mol%) were placed in a Schlenk tube. Then, 20 mL of dry dimethylformamide (DMF) was added, and the solution was subjected to freeze–pump–thaw cycles to remove dissolved oxygen. Next, 2 mL of a degassed aqueous solution of potassium carbonate (2 M) was added to the mixture. The reaction mixture was vigorously stirred at 140 °C under an inert atmosphere for 3 days. The reaction mixture was allowed to cool to room temperature and then diluted with 50 mL of cold methanol, and the green-colored precipitate was collected by filtration. The precipitate was washed with methanol, water, acetone, and dichloromethane; rigorously washed by Soxhlet extraction with methanol, acetone, and ethyl acetate; and then dried under vacuum at 120 °C overnight to produce CPP-P2 (60% yield) as a green solid.

3.3. Computational Methods

The computational modeling was accomplished using density functional theory (DFT) and implemented with the pseudopotential code SIESTA [26] as previously used in our work on the ORR of nitrogen-doped graphene [23]. All calculations were performed using the generalized gradient approximation (GGA-PBE) including spin polarization [27], while including a van der Waals correction [28]. Full optimization of the atomic positions was performed. During this optimization, the ion cores were described by norm-conserving nonrelativistic pseudopotentials [29], with cutoff radii of 1.14, 1.48, 1.47, and 1.25 atomic units for C, N, O, and H, respectively; the wave functions were expanded with a double- ζ plus polarization basis of localized orbitals for non-hydrogen atoms and with a double- ζ basis for H. The optimization of the force and total energy were performed with accuracies of 0.04 eV/Å and 1 meV, respectively.

The calculation of the free energy was performed using a previously developed method [25,29] for platinum-based catalysis using the formula $G = \Delta H + neU + EZP$, where ΔH is the energy difference between the total energies at the initial and final stages of each step of the ORR, e is the electron charge, U is the equilibrium potential, n is the number of OH^- groups produced at the considered step in the reaction, and EZP is the zero-point energy correction. The value of U (0.89 eV) is standard for the process in basic media. The zero-point energy corrections are the same as previously used [25,29]. An external energy field that could change the chemisorption energy [30] was not included in our simulation.

4. Conclusions

We demonstrated the synthesis of a pyrazine- and pyridine-containing conjugated porous polymer. As a proof of concept, we used the polymer as a heterogeneous catalyst for oxygen reduction. A detailed mechanism for the four-electron ORR was proposed on the basis of DFT calculations. A possible pathway for the reaction includes the decomposition of the oxygen molecule on the nearest pyrazine site with the further transformation of N=O to N-OH. Theoretical calculations also established the lower free energy of the ORR steps for less-densely packed structures.

Supplementary Materials: The following are available online at <http://www.mdpi.com/2073-4344/10/11/1224/s1>, Scheme S1: Schematic representation of synthesis of CPOP-P2, Figure S2: Free energy of the ORR involving two pyrazine sites for two different types of CPP-P2 packing (Figure 6).

Author Contributions: Data collection and writing—original draft preparation, S.B.; writing—review, S.R.H. and M.A.K.; references and downloads, C.L. and H.I.J.; writing—review and supervision, S.L. and M.S.T.; writing—review and editing, supervision, and project administration, B.R.L. and D.W.B.; writing—review and supervision, H.C. All authors have read and agreed to the published version of the manuscript.

Funding: This work was funded by National Research Foundation (NRF) of Korea (Grants NRF-2020R1A4A1018163) under the program of Basic Research Laboratory (BRL). This research was partially funded by the Ministry of Science and Higher Education of the Russian Federation (through the basic part of the government mandate, Project No. FEUZ-2020-0060).

Acknowledgments: This work was supported by the research fund of Hanyang University (HY-2018). S.B. is also thankful for financial support from a DST-SERB NPDF fellowship (PDF/2019/001343/CS).

Conflicts of Interest: The authors declare no conflict of interest.

References and Notes

1. Adler, S.B. Factors Governing Oxygen Reduction in Solid Oxide Fuel Cell Cathodes. *Chem. Rev.* **2004**, *104*, 4791–4844. [[CrossRef](#)] [[PubMed](#)]
2. Staffell, I.; Scamman, D.; Velazquez Abad, A.; Balcombe, P.; Dodds, P.E.; Ekins, P.; Shah, N.; Ward, K.R. The Role of Hydrogen and Fuel Cells in the Global Energy System. *Energy Environ. Science* **2019**, *12*, 463–491. [[CrossRef](#)]
3. Bu, L.; Ding, J.; Guo, S.; Zhang, X.; Su, D.; Zhu, X.; Yao, J.; Guo, J.; Lu, G.; Huang, X. A General Method for Multimetallic Platinum Alloy Nanowires as Highly Active and Stable Oxygen Reduction Catalysts. *Adv. Mater.* **2015**, *27*, 7204–7212. [[CrossRef](#)] [[PubMed](#)]
4. Cho, K.; Han, S.H.; Suh, M.P. Copper–organic Framework Fabricated with CuS Nanoparticles: Synthesis, Electrical Conductivity, and Electrocatalytic Activities for Oxygen Reduction Reaction. *Angew. Chem. Int. Ed.* **2016**, *55*, 15301–15305. [[CrossRef](#)]
5. Jaouen, F.; Proietti, E.; Lefevre, M.; Chenitz, R.; Dodelet, J.P.; Wu, G.; Chung, H.T.; Johnston, C.M.; Zelenay, P. Recent Advances in Non-precious Metal Catalysis for Oxygen-Reduction Reaction in Polymer Electrolyte Fuel cells. *Energy Environ. Sci.* **2011**, *4*, 114–130. [[CrossRef](#)]
6. Zhang, J.; Zhao, Z.; Xia, Z.; Dai, L. A metal-free Bifunctional Electrocatalyst for Oxygen Reduction and Oxygen Evolution Reactions. *Nat. Nanotechnol.* **2015**, *10*, 444. [[CrossRef](#)]
7. Guo, D.; Shibuya, R.; Akiba, C.; Saji, S.; Kondo, T.; Nakamura, J. Active Sites of Nitrogen-doped Carbon Materials for Oxygen Reduction Reaction Clarified using Model Catalysts. *Science* **2016**, *351*, 361–365. [[CrossRef](#)]
8. Duan, J.; Chen, S.; Jaroniec, M.; Qiao, S.Z. Heteroatom-Doped Graphene-Based Materials for Energy-Relevant Electrocatalytic Processes. *ACS Catal.* **2015**, *5*, 5207–5234. [[CrossRef](#)]
9. Singh, S.K.; Takeyasu, K.; Nakamura, J. Active Sites and Mechanism of Oxygen Reduction Reaction Electrocatalysis on Nitrogen-Doped Carbon Materials. *Adv. Mater.* **2018**. [[CrossRef](#)]
10. Lee, S.H.; Kim, J.; Chung, D.Y.; Yoo, J.M.; Lee, H.S.; Kim, M.J.; Mun, B.S.; Kwon, S.G.; Sung, Y.E.; Hyeon, T. Design Principle of Fe-N-C Electrocatalysts: How to Optimize Multimodal Porous Structures? *J. Am. Chem. Soc.* **2019**, *141*, 2035–2045. [[CrossRef](#)]
11. Lv, Q.; Si, W.; He, J.; Sun, L.; Zhang, C.; Wang, N.; Yang, Z.; Li, X.; Wang, X.; Deng, W.; et al. Selectively Nitrogen-doped Carbon Materials as Superior Metal-free Catalysts for Oxygen Reduction. *Nat. Commun.* **2018**, *9*, 3376. [[CrossRef](#)]

12. Wei, Q.; Tong, X.; Zhang, G.; Qiao, J.; Gong, Q.; Sun, S. Nitrogen-doped Carbon Nanotube and Graphene Materials for Oxygen Reduction Reactions. *Catalysts* **2015**, *5*, 1574–1602. [[CrossRef](#)]
13. Roy, S.; Bandyopadhyay, A.; Das, M.; Ray, P.P.; Pati, S.K.; Maji, T.K. Redox-active and Semi-conducting Donor–acceptor Conjugated Microporous Polymers as Metal-free ORR catalysts. *J. Mater. Chem. A* **2018**, *6*, 5587–5591. [[CrossRef](#)]
14. Xu, Y.; Jin, S.; Xu, H.; Nagai, A.; Jiang, D. Conjugated Microporous Polymers: Design, Synthesis and Application. *Chem. Soc. Rev.* **2013**, *42*, 8012–8031. [[CrossRef](#)]
15. Bandyopadhyay, S.; Pallavi, P.; Anil, A.G.; Patra, A. Fabrication of Porous Organic Polymers in the form of Powder, Soluble in Organic Solvents and Nanoparticles: A Unique Platform for Gas Adsorption and Efficient Chemosensing. *Polym. Chem.* **2015**, *6*, 3775–3780. [[CrossRef](#)]
16. Slater, A.G.; Cooper, A.I. Porous Materials Function-led Design of New Porous Materials. *Science* **2015**, *348*, 6238. [[CrossRef](#)]
17. Zhang, M.; Ming, J.; Zhang, W.; Xie, J.; Lin, P.; Song, X.; Chen, X.; Wang, X.; Zhou, B. Porous Organic Polymer-Derived Fe2P@N,P-Codoped Porous Carbon as Efficient Electrocatalysts for pH Universal ORR. *ACS Omega* **2020**, *5*, 7225–7234. [[CrossRef](#)]
18. Xue, Q.; Li, W.; Dou, J.; Song, W.; Ming, J.; Bian, W.; Guo, Y.; Li, X.; Zhang, W.; Zhou, B. Porous Organic Polymers as Fire-Resistant Additives and Precursors for Hyperporous Carbon towards Oxygen Reduction Reactions. *ChemistryOpen* **2020**, *9*, 593. [[CrossRef](#)]
19. Bandyopadhyay, S.; Boukhvalov, D.W.; Nayak, A.K.; Ha, S.R.; Shin, H.J.; Kwon, J.; Song, T.; Choi, H. Redox Active Nitrogen-containing Conjugated Porous Polymer: An Organic Heterogeneous Electrocatalysts for Oxygen Reduction Reaction. *Dye Pigment.* **2019**, *170*, 107557. [[CrossRef](#)]
20. Trivedi, M.; Tallapragada, R.; Branton, A.; Trivedi, D.; Nayak, G.; Mishra, R.; Jana, S. Characterization of Physical, Spectroscopic and Thermal Properties of Biofield Treated Biphenyl. *Am. J. Chem. Eng.* **2015**, *3*, 58–65. [[CrossRef](#)]
21. Chang, D.W.; Choi, H.-J.; Baek, J.-B. Wet-chemical Nitrogen-doping of Graphene Nanoplatelets as Electrocatalysts for the Oxygen Reduction Reaction. *J. Mater. Chem. A* **2015**, *3*, 7659–7665. [[CrossRef](#)]
22. Radovic, L.R.; Suarez, A.; Vallejos-Burgos, F.; Sofo, J.O. Oxygen Migration on the Graphene Surface. 2. Thermochemistry of basal-plane Diffusion (hopping). *Carbon* **2011**, *49*, 4226. [[CrossRef](#)]
23. Boukhvalov, D.W.; Son, Y.-W. Oxygen Reduction Reactions on Pure and Nitrogen-doped Graphene: A First-principles Modeling. *Nanoscale* **2012**, *4*, 417. [[CrossRef](#)]
24. Duan, Z.; Henkelman, G. Theoretical Resolution of the Exceptional Oxygen Reduction Activity of Au(100) in Alkaline Media. *ACS Catal.* **2019**, *9*, 5567. [[CrossRef](#)]
25. Hansen, H.A.; Rossmesl, J.; Nørskov, J. Surface Pourbaix Diagrams and Oxygen Reduction Activity of Pt, Ag and Ni (111) Surfaces Studied by DFT. *Phys. Chem. Chem. Phys.* **2008**, *10*, 3722. [[CrossRef](#)]
26. Perdew, J.P.; Burke, K.; Ernzerhof, M. Generalized Gradient Approximation made Simple. *Phys. Rev. Lett.* **1996**, *77*, 3865–3868. [[CrossRef](#)]
27. Romaán-Peérez, G.; Soler, J.M. Efficient Implementation of a Van der Waals Density Functional: Application to Double-wall Carbon Nanotubes. *Phys. Rev. Lett.* **2009**, *103*, 096102. [[CrossRef](#)]
28. Troullier, O.N.; Martins, J.L. Efficient Pseudopotentials for Plane-wave Calculations. *Phys. Rev. B* **1991**, *43*, 1993. [[CrossRef](#)]
29. Nørskov, J.; Rossmesl, J.; Logadottir, A.; Lindqvist, L.; Kitchin, J.R.; Bligaard, T.; Jonsson, H. Origin of the Overpotential for Oxygen Reduction at a Fuel-cell Cathode. *J. Phys. Chem. B* **2004**, *108*, 17886. [[CrossRef](#)]
30. Ao, Z.M.; Peeters, F.M. Electric Field Activated Hydrogen Dissociative Adsorption to Nitrogen-doped Graphene. *J. Phys. Chem. C* **2010**, *114*, 14503. [[CrossRef](#)]

Publisher’s Note: MDPI stays neutral with regard to jurisdictional claims in published maps and institutional affiliations.



© 2020 by the authors. Licensee MDPI, Basel, Switzerland. This article is an open access article distributed under the terms and conditions of the Creative Commons Attribution (CC BY) license (<http://creativecommons.org/licenses/by/4.0/>).